V European Conference on Computational Fluid Dynamics
ECCOMAS CFD 2010
J. C. F. Pereira and A. Sequeira (Eds)
Lisbon, Portugal,14-17 June 2010

H- AND P- ADAPTIVE INCOMPRESSIBLE FLOW SOLUTIONS ON CARTESIAN GRIDS USING LEAST SQUARES SPECTRAL ELEMENT METHOD

Altug Ozcelikkale*, Cuneyt Sert†

*†Department of Mechanical Engineering,
Middle East Technical University,
Ankara 06531 Turkey
*e-mail: e144689@metu.edu.tr
†e-mail: csert@metu.edu.tr

Key words: Incompresible flow; Adaptive refinement; Cartesian grid; Least squares; Spectral Element Method

Abstract. *Use of numerical solutions to flow phenomena has become increasingly common among non-engineering disciplines such as medical sciences. This increasing interest can be promoted by the ability of solvers to obtain accurate numerical solutions without the need for expertise in some specific subjects such as grid generation or automatic grid adaptation. In this work, an incompressible flow solver is developed with emphasis on generating the initial computational grid automatically and obtaining the solution accurately, fast and efficiently with minimum user intervention. For this purpose, a non-conforming Cartesian grid (NCG) structure is used. The 2-dimensional, laminar, incompressible Navier-Stokes equations are solved by a spectral element method based on least squares principles, which offers significant advantages over traditionally employed Galerkin formulations for flow problems. Convergence to the solution is automated by a p-type adaptive refinement strategy based on least squares functional error estimate. Two solution procedures that are employed in least squares spectral element method (LSSEM) literature, matrix-free method and Schur complement decomposition are compared qualitatively based on CPU and memory performance. The solver is tested by solving various benchmark problems and comparing the results with past studies. It is shown that mass conservation performance of LSSEM can be improved effectively by using p-type adaptive refinement.*

1 INTRODUCTION

Use of computational approaches to solve flow problems are becoming more common in non-engineering disciplines such as medicine. The application areas of numerical flow solution techniques in these disciplines can be further extended by enabling people with little or no knowledge in numerical methods use such techniques to solve their problems with ease and success. Such an idea can be realized by the development of numerical softwares that have the ability to obtain an accurate solution fast and efficiently with minimum user intervention. In this context, adaptive grid (mesh) refinement (AMR) strategies came forward as a way of automating the solution procedure.

Recent AMR studies focus on use of non-conforming Cartesian Grids (NCG). NCG offers an elegant way to discretize domains with complex-moving boundaries[1]. Moreover, NCG have a flexible grid structure which is allows for efficient implementation of AMR[2]. A great amount of work is done in this subject by using NCG with low order finite volume methods, referred as immersed boundary methods where the boundaries remain immersed in the regular computational grid and the cells cut by the boundaries are treated by singular forces[3]. In contrary, use of finite element methods (FEM) and high order spectral element methods (SEM) with NCG are rare in literature. In this study, a SEM solver with the ability to work on NCG is developed to address this gap.

It is possible to use different variational formulations to obtain different types of finite and spectral element methods. The SEM solver presented in this study is based on least squares (LS) variational formulation[4] which is reported to offer significant advantages over the classical Galerkin variational formulation for the solution of flow problems[5]. However, LS methods have also some disadvantages. Most importantly, FEM and SEM based on LS principles are reported to have poor mass conservation performance for flows with inflow and outflow[6,7]. In this study, it is shown that the mass conservation properties of the least squares spectral element method (LSSEM) can be improved by using a p-adaptive refinement strategy.

2 LEAST SQUARES FORMULATION

Least squares variational formulation for the numerical solution of partial differential equations was first introduced by Bramble and Schatz [4]. Later it was offered by Jiang [5] as a better alternative to classical Galerkin formulations for flow problems since it allows for the use of equal order approximations for all unknowns of the problem without violating the LBB condition, can solve advection dominated problems accurately without resorting to upwinding and results in a positive-definite linear system of equations that can be solved by preconditioned conjugate gradient solvers efficiently.[5] It has also some disadvantages. For instance, in order to use LS formulation with practical basis expansions that merely require $\mathbb{C}^0$ continuity of the solution across elements, these equations must be cast into an equivalent set of first order equations[8]. This procedure leads to solution of additional unknowns and results in extra computational resources. Nevertheless, in the case of flow

problems the additional unknowns are of physical interest and the extra effort is not totally in vain. Additionally, LSFEM and LSSEM are reported to exhibit poor mass conservation performance[6]. This issue is addressed extensively in the literature[6,9–11]. See section 5.3 for additional discussion on mass conservation.

For completeness, the LS formulation is derived for a model boundary value problem here.

$$\mathcal{L}u = f \qquad \text{on } \Omega \tag{1a}$$

$$\mathcal{B}u = g \qquad \text{on } \partial\Omega \tag{1b}$$

where Ω is a closed domain bounded by $\partial\Omega$, $\mathcal{L}$ is a first order linear partial differential operator defined on Ω, $\mathcal{B}$ is an algebraic boundary operator defined on $\partial\Omega$, u is the unknown, f is the forcing function and g is the boundary value function. Restricting our attention to real valued functions, it is assumed that f is a member of the space of square integrable functions on Ω, i.e. $f \,\epsilon\, \mathbb{L}_2(\Omega)$ and u is a continuous function with piecewise continuous first partial derivatives on Ω, i.e. $u \,\epsilon\, \mathbb{H}_1(\Omega)$.

We define the residual of eqn.(1a) as $R = \mathcal{L}u - f$. The residual is not identically equal to zero on the whole problem domain unless u is the exact solution. In least squares method, the approximate solution is required to minimize the square of the L_2-norm of the residual $\|R\|^2_{\mathbb{L}_2}$, which is referred as the least squares functional $\mathcal{I}$. Minimization is done by taking the first variation of $\mathcal{I}$ and equating it to zero. Following the procedure and rearranging the terms, the least squares formulation in continuous form is obtained.

Seek $u \,\epsilon\, \mathbb{H}_1(\Omega)$ such that

$$\int_\Omega (\mathcal{L}v)^T (\mathcal{L}u)\, d\Omega = \int_\Omega (\mathcal{L}v)^T f\, d\Omega \quad \forall v \,\epsilon\, \mathbb{H}_1,\ v = 0 \text{ on } \partial\Omega \tag{2a}$$

$$\mathcal{B}u = g \quad \text{on } \partial\Omega \tag{2b}$$

where v is the variation of u. Note that $v = 0$ on the entire boundary since the boundary operator $\mathcal{B}$ is algebraic implying essential boundary conditions only. This is an advantage of applying least squares method to first order equations. Since no weak form is used, only essential boundary conditions are imposed in least squares formulation.

The formulation can be extended to solution of a set of first order differential equations with multiple unknowns. See, for instance, Jiang [5] for details.

3 GOVERNING EQUATIONS

In this study incompressible Navier-Stokes equations are solved for the numerical prediction of two-dimensional, laminar flows.

$$\nabla \cdot \mathbf{u} = 0 \qquad \text{(Continuity)} \tag{3a}$$

$$\frac{\partial \mathbf{u}}{\partial t} + \mathbf{u} \cdot \nabla \mathbf{u} + \frac{1}{\rho} \nabla p - \nu \nabla^2 \mathbf{u} = \mathbf{f} \qquad \text{(Momentum)} \tag{3b}$$

In order to solve eqn.(3) with LSSEM, it must be converted into an equivalent set of first order differential equations by introducing an additional unknown. The vorticity $\boldsymbol{w}$ can be used for this purpose. With introduction of the vector identity

$$\nabla^2\mathbf{u} = -\nabla \times (\nabla \times \mathbf{u}) + \nabla(\nabla \cdot \mathbf{u}) \tag{4}$$

and the divergence free constraint (3a) in eqn.(3)

$$\nabla \cdot \mathbf{u} = 0 \qquad \text{(Continuity)} \tag{5a}$$

$$\frac{\partial \mathbf{u}}{\partial t} + \mathbf{u} \cdot \nabla\mathbf{u} + \frac{1}{\rho}\nabla p + \nu \nabla \times \boldsymbol{\omega} = \mathbf{f} \qquad \text{(Momentum)} \tag{5b}$$

$$\boldsymbol{\omega} - \nabla \times \mathbf{u} = 0 \qquad \text{(Vorticity Definition)} \tag{5c}$$

Eqn.(5) is referred as the velocity-pressure-vorticity formulation of Navier-Stokes equations.[5]

For the 2-dimensional form of eqn.(5) considered in Cartesian coordinates, the unknowns are x and y-components of velocity, u and v, pressure p and the z-component of vorticity w. For the approximation of unknowns a space time decoupled approach is followed. A spectral element method is used for the spatial approximation while an α-family time integration scheme[12] is used for temporal approximation of the unknowns. The convective terms are linearized by Newton linearization.

4 IMPLEMENTATION

A spectral element method based on least squares formulation (LSSEM) is used in the spatial approximation of unknowns in eqn.(5). Spectral element method (SEM) utilizes a combination of the sub-domain division approach of finite element methods (FEM) and high order approximation of spectral methods (SM)[13]. As in FEM, the domain is divided into several sub-domains (elements). By this way complex geometries can be handled appropriately. As the element sizes get smaller the unknown can be sufficiently represented over each element by a basis expansion. Again considering the model problem given by eqn.(1),

$$u^e(\mathbf{x}) \approx u^e_{hp}(\mathbf{x}) = \sum_{i=1}^{N} \hat{u}^e_i \, \phi^e_i(\mathbf{x}) \tag{6}$$

where u^e is the solution on an element sub-domain Ω^e and u^e_{hp} is the SEM approximation to it. $\mathbf{x}$ is a point contained in the domain or on its boundary. N is the order of expansion, $\hat{u}^e_i$ are the elemental unknown coefficients and $\phi^e_i(x)$ are the elemental basis functions. For the elemental basis functions, orthogonal set of Jacobi polynomials such as Chebyshev or Legendre polynomials (modal expansion) or Lagrange interpolating polynomials (nodal expansion) can be used. For 2 and 3-dimensional problems, the basis functions can be constructed by using a tensor product of those set of polynomials. To develop LSSEM, integrals in (2) are broken down into integrals over elemental sub-domains and elemental

approximations (6) are substituted in places of u and v. This procedure results in an N×N system of equations for each element,

$$\mathbf{K^e}\,\mathbf{U^e} = \mathbf{F^e} \tag{7}$$

where

$$\mathbf{K^e_{ij}} = \int_{\Omega^e} (\mathcal{L}\phi_i)^T\,(\mathcal{L}\phi_j)\;d\Omega^e \qquad \text{and} \quad \mathbf{F^e_i} = \int_{\Omega^e} (\mathcal{L}\phi_i)^T\,\mathbf{f}\,d\Omega^e \tag{8}$$

The elemental unknown vector $\mathbf{U^e}$ is composed of the expansion coefficients $\hat{u}_i^e$. The elemental systems (7) are assembled into a global system and solved accordingly.

In this study, tensor products of Lagrange interpolating polynomials defined on a Gauss-Lobatto-Legendre (GLL) interpolation grid is used as the basis functions. The Lagrange interpolating polynomials have the cardinality property leading to use of unknowns values at the nodal points defined by the GLL grid as the unknown coefficients. This feature simplifies the implementation. The integrals in (8) are evaluated with Gauss-Lobatto integration rule which is also based on the GLL grid. This choice of interpolation grid and numerical quadrature leads to coincident grid nodes and quadrature points which reduces the computational complexity of the elemental system calculation.

Use of LSSEM on non-conforming Cartesian grid leads to two types of non-conformities in element interfaces. h-type non-conforming interfaces (figure 1a) occur where an element becomes neighbor to more than one element at a single edge. That is, the interfacing elements are geometrically non-conforming. h-type non-conformities are a direct result of using a non-conforming Cartesian grid. Another type of non-conformity is the p-type non-conformity that arises due to the use of high order expansions on individual elements. In p-type non-conforming interfaces (figure 1b) two elements are geometrically conforming at the adjacent edges but they use different orders of expansions to approximate the unknowns on those edges. The solver developed in this study handles both types of non-conformities by the constrained approximation method.[14] In constrained approximation method, one of the interfacing edges are declared as *active* and the nodal unknowns on this edge are used in global assembly process. The nodal unknowns on the other (*passive*) edge(s) are not a part of global solution. For elemental operations, they are interpolated from the unknowns on the *active* edge. Degree of the interpolation is the same as the expansion order used on the *active* edge. In this study, activeness of edges at an h-type non-conformity are decided according to *long rule* where the edge which is longer is made active. Similarly, activeness of edges at a p-type non-conformity, are decided according to *minimum rule* where the edge with lower expansion order is set as active. For the details of constrained approximation method, one can refer to Sert and Beskok [15].

As in the case of non-conformities, use of LSSEM on NCG provides two choices for adaptive refinement strategy. In h-type refinement, elements are divided into smaller elements without changing the expansion orders until the solution is adequately represented over each element. In p-type refinement, element size is kept fixed and expansion orders are increased. hp-type refinement where both h- and p-type refinement are employed is

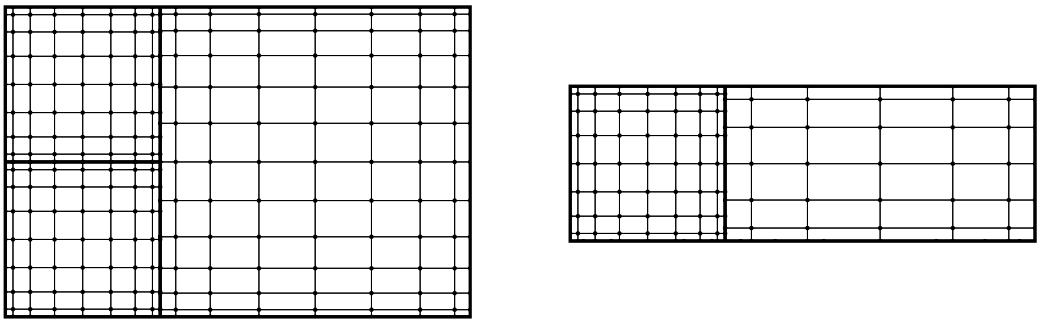

(a) h-type nonconformity (b) p-type nonconformity

Figure 1: Types of non-conforming interfaces encountered in LSSEM with NCG

also possible. Implementing h-type adaptive refinement to the solver is an issue worked on in the time of writing this text. The solver presented here can perform p-type adaptive refinement on conforming and non-conforming grids. The adaptive refinement criteria is based on the value of the least squares functional over each element[16]. An efficient use of computational resources can be realized by keeping the value of least squares functional over each element between prescribed error bounds. Therefore p-type adaptive refinement is performed to obtain and maintain the following condition

$$\varepsilon_{min} \leq \frac{\mathcal{I}_e}{A_e} \leq \varepsilon_{max} \tag{9}$$

Typical values for the error bounds range from 10^{-6} to 10^{-9}. It is also possible to normalize the element area averaged least squares functional $\mathcal{I}_e/A_e$ with some norm of the element unknown vector though this approach is not employed in the current study. The adaptive refinement procedure is carried across time steps.

Steady state solutions presented in section 5 were obtained by marching in time. For the α parameter in the time integration scheme $\alpha = 2/3$, corresponding to second order accurate Galerkin scheme[12] is used. Solutions with Crank-Nicholson scheme ($\alpha = 0.5$) are also obtained. However those solutions show temporal oscillations in pressure values across the domain. On the other hand, solutions obtained by the Galerkin scheme are free of such oscillations.

The assembly of the elemental systems into a global system is not necessarily performed physically. The system can be solved by a Jocobi preconditioned conjugate gradient method through an element-by-element procedure where a global coefficient matrix is never constructed.[16] In the so-called *matrix-free method*[17], the memory requirements are further reduced by not keeping the elemental systems in the memory, instead recalculating them at each linear solver iteration. Such an approach is especially required when solving large 3-dimensional problems where forming the global system or keeping the elemental system in memory require excessive resources. The design of the solver

presented here is currently focused on solving 2-dimensional problems. For those problems, keeping the elemental systems in memory through the linear solution process is still feasible. Since the elemental systems are calculated only once for the linear solution, such an approach is especially efficient as far as computation time is concerned. Current solver uses this approach together with *static condensation* [18] to further reduce the computation time and memory requirements. In static condensation, solution of elemental boundary and interior unknowns are decoupled from each other by forming the Schur's complement of the elemental system. By this way, solution of the elemental system is replaced by the solution of two smaller systems. Static condensation reduces the use of computational resources for 2-dimensional problems. However, preparation of elemental systems by static condensation for the solution step involves computationally intensive tasks such as a positive-definite matrix inversion. Therefore it may not be feasible to use static condensation with a memory optimizing approach such as matrix-free method. The matrix-free method may be the only option for the solution of 3-dimensional problems with element-by-element procedure.

5 BENCHMARK SOLUTIONS

In this section, the solver introduced in previous sections is validated by solving various flow problems.

5.1 Kovasznay Flow

Kovasznay flow was originally presented by Kovasznay [19]. It's exact solution is used to verify convergence characteristics of incompressible Navier-Stokes solvers. This problem is solved to verify the spectral convergence of the solver for various grid configurations.

Kovasznay flow is solved on a rectangular domain: $[-0.5, 1]\times[1, 1.5]$. The exact solution is

$$u_e = 1 - e^{\lambda x} cos\,(2\pi y) \tag{10a}$$

$$v_e = \frac{\lambda}{2\pi}\, e^{\lambda x} sin\,(2\pi y) \tag{10b}$$

$$p_e = \frac{1}{2}\left(1 - e^{2\lambda x}\right) \tag{10c}$$

where $\lambda = 1/2\nu - \left[(1/4\nu^2) + 4\pi^2\right]^{1/2}$, v being the kinematic viscosity. Stream function contours of the exact solution are shown in figure 2a.

In order to study the convergence properties of the solver, solutions on conforming, p-type non-conforming and h-type non-conforming grids are performed as follows:

1. Conforming Grid: In this study, grid 1, illustrated in figure 2b is used. This grid has 8 elements. Same expansion order, p is used for all elements and in both space dimensions, resulting in conforming element interfaces.

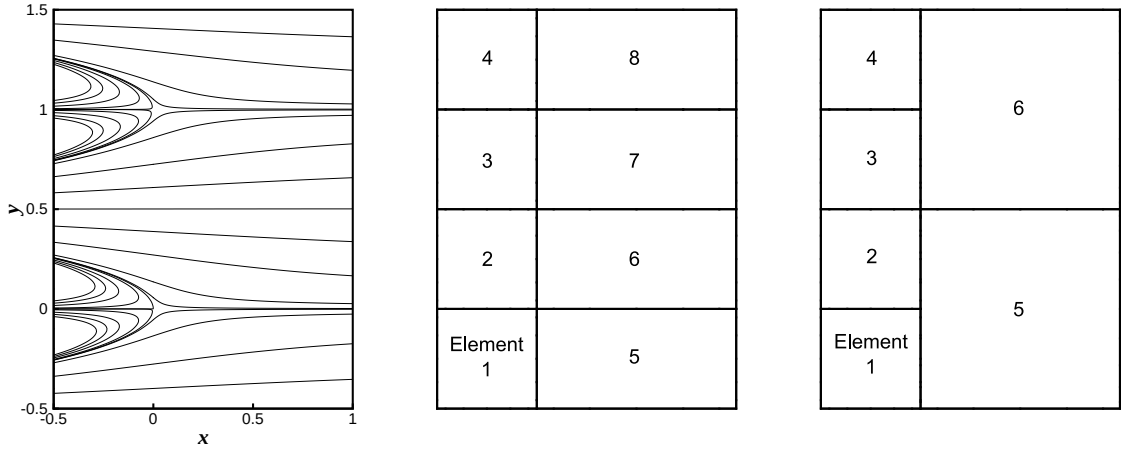

(a) Streamlines (b) Grid 1 (c) Grid 2

Figure 2: Kovasznay flow: Exact solution and the computational grids used in this study

2. p-type Non-conforming Grid: Again, grid 1 is used. However this time, expansion orders of elements are altered such that elements 1, 4, 6 and 7 have expansion orders p while elements 2, 3, 5 and 8 have expansion orders $p-2$. Same expansion order is used in both space dimensions. This setup results in p-type non-conforming interfaces.

3. h-type Non-conforming Grid: In this study, grid 2, illustrated in figure 2c is used. Here, 2 h-type non-conforming interfaces lying in y-direction are present. Elements on the left half of the domain have expansion orders p in both space dimensions. The two large elements on the right hand side also have expansion order p in the x-direction. $p+4$ is used in y-direction to compensate for the large element size in that direction.

For all the grids described above, a series of solutions are performed for various expansion orders by starting with $p = 6$ and incrementing by 2 until $p = 14$. For non-conforming grids, the expansion order of the individual elements is not a representative value of the expansion order of the whole grid since it varies from one element to other. Therefore here the number of degree of freedom used to approximate each of the unknowns, ndf is used as a measure of expansion order. In figure 3, a semi-log plot of maximum-norm error in x-velocity, $\|u_e - u\|_\infty$ against $\sqrt{ndf}$ is presented. The use of $\sqrt{ndf}$ as the independent variable ensures that the spectral convergence trend is displayed as a straight line on semi-log plot. Straight line patterns in figure 3 indicate that spectral convergence is achieved for all three grid configurations regardless of the presence of p- and h-type non-conformities.

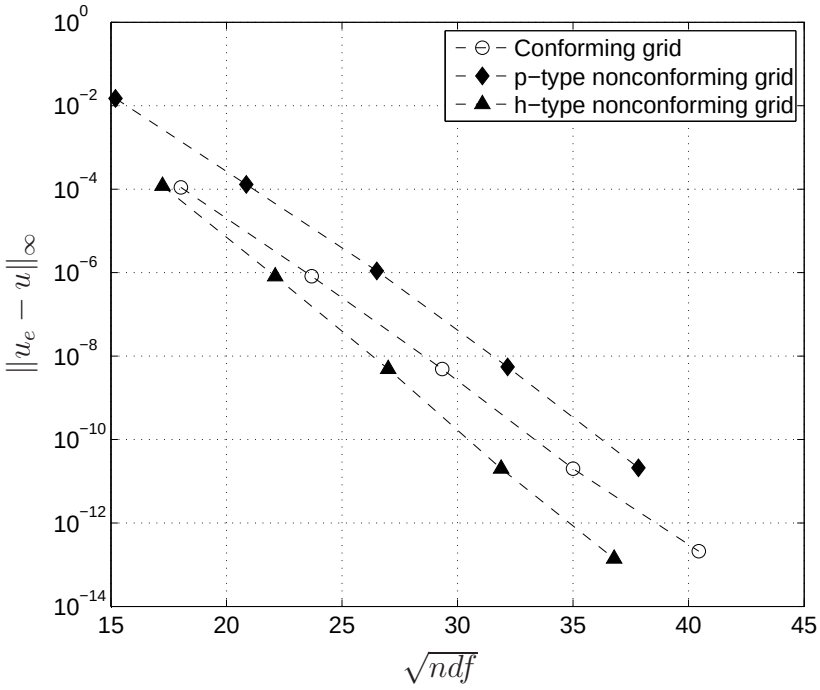

Figure 3: Convergence trends for conforming, p-type nonconforming and h-type nonconforming grids for Kovasznay flow

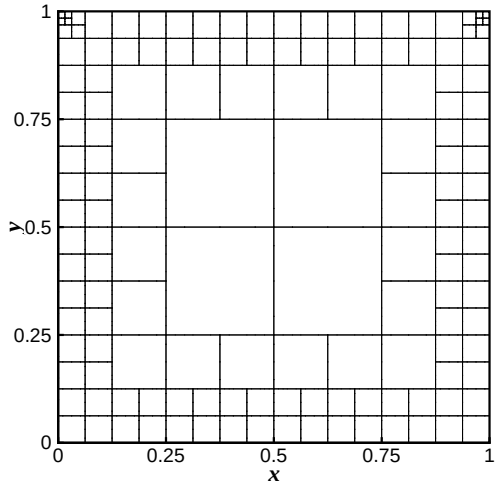

Figure 4: Lid-driven cavity: computational grid

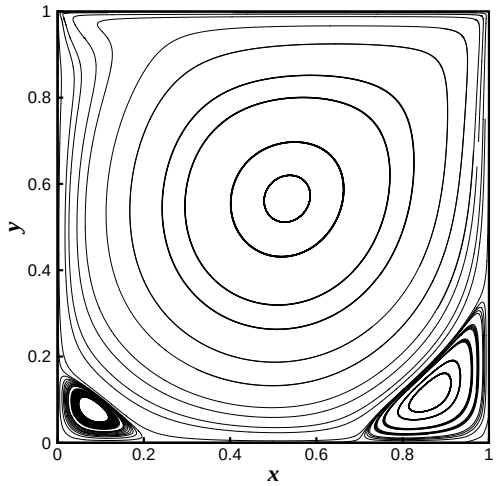

Figure 5: Lid-driven cavity: Stream function contours

5.2 2-Dimensional Lid-Driven Cavity Flow

Another popular incompressible flow problem is the shear driven flow inside a 2-dimensional square cavity. The flow is induced by an infinite lid at the top of the cavity, pulled in x-direction with constant velocity. The main flow features are a large central vortex in the middle of the cavity and small corner vortices whose size and number change with Re number.

This problem is solved with a non-conforming Cartesian grid to illustrate the ability of the solver to work with h-type non-conforming grids in practice. No adaptive refinement is employed. All elements have expansion orders $p = 4$ in both directions. It is worth to mention that x-velocity is discontinuous at upper corners resulting in a singular solution for velocity there. High-order methods are sensitive to such singularities by nature. Therefore it is desirable to minimize the effect of these singularities on the solution. It is possible to subtract the singular solutions at the corners to end up with a smooth solution[20] or to solve a regularized version of the problem where the velocity boundary condition is smoothed near corners[21]. Here, the computational grid is refined at those corners to isolate the effect of singularities to surrounding small elements. The size of the elements in the rest of the grid are not affected due to use of non-conforming Cartesian grid. The grid used in the solution is illustrated in figure 4.

The presented solution is performed for $Re = 1000$. For visual acquisition, stream function contours are presented in figure 5. The position of the central vertex and the sizes of the corner vortices are captured properly. Figures 6 and 7 show the x and y-velocities taken

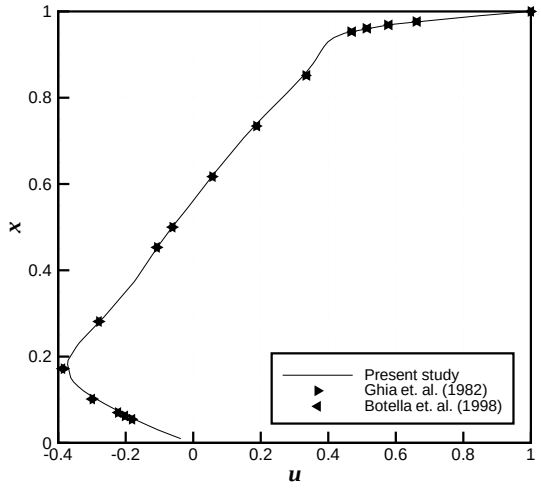

Figure 6: Lid-driven Cavity: x-velocity profile across the vertical centerline

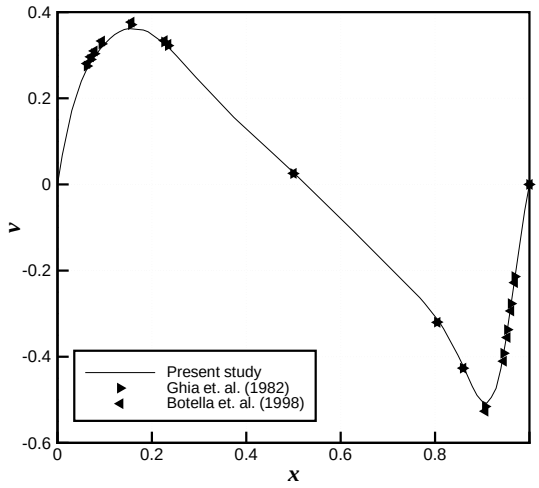

Figure 7: Lid-driven Cavity: y-velocity profile across the horizontal centerline

from the vertical and the horizontal centerlines of the domain. The profiles are in well agreement with the multi-grid finite difference solution of Ghia et al. [22] and Chebyshev spectral solution of Botella and Peyret [20]. It is seen that a practical problem can be solved with LSSEM on a non-conforming Cartesian grid accurately.

5.3 Laminar Flow Past Cylinder in a Channel

The flow of interest is the laminar flow in a channel where the flow is partially blocked by a large circular cylindrical obstacle. This problem and its variants are encountered frequently in the mass conservation studies of least squares formulation. The issue of LS formulation showing poor mass conservation performance compared to the Galerkin formulation was first reported by Chang and Nelson [6]. Several remedies that modify the least squares formulation[6,9–11] were suggested since that time. More recently, it was observed that the mass conservation performance can be improved by increasing the expansion order alone, without modifying the formulation, in the case of least squares spectral collocation method[23].

In this study, the problem is solved on a rectangular channel $[-11, 15] \times [-1, 1]$. A cylinder with diameter $D = 1$ is placed at the origin. No slip boundary conditions are applied at the upper and lower channel walls and the surface of the cylinder. A uniform inflow $u = 1, v = 0$ is prescribed at $x = -11$ to stay consistent with the literature[11] and an outflow boundary condition with tangential velocity and pressure set to zero is enforced at the downstream boundary. The resulting Reynolds number based on cylinder diameter

is 40 for which a steady, laminar solution exists. It is worth to mention that while the solver is designed to work with a non-conforming adaptive Cartesian grid eventually, it is also capable of handling arbitrary quadrilateral elements. Here, the computational grid consists of 32 quadrilateral elements. The elements near the cylinder have curved edges to represent the cylinder geometry accurately. The cylinder geometry is provided as line-segmented data from which the coordinates of the nodal points on the related edges are interpolated using an 8^{th} degree Lagrange interpolation. Coordinates of the rest of the nodes and the Jacobians of the elements with curved edges are calculated using Gordon-Hall trans-finite interpolation[24].

Two solutions are obtained using the described configuration. First, the problem is solved by setting element expansion orders to $p = 6$. p-type adaptive refinement is not employed, resulting in a conforming grid. The details of this grid, referred as the non-adaptive grid, and the associated solution are presented in figure 8a. It is seen that the length of recirculation zone behind the cylinder is underestimated by the non-adaptive grid. This region should extend beyond $x = 1$ for a mass conserving solution[11]. The second solution is obtained by using the same grid as the initial grid and employing p-type adaptive refinement. Expansion orders as high as 20 and as low as 4 are allowed. The refinement criteria is to keep area averaged least squares functional for each element within the interval $[10^{-9}, 10^{-6}]$. The final grid reached at steady state, referred as the adaptive grid, and the associated solution are presented in figure 8b. It is observed that, this time the recirculation zone expands well beyond $x = 1$ up to $x = 1.35$.

For a more quantitative comparison, x-velocity profile at the vertical cross-section between the cylinder and lower channel wall at which maximum velocity occurs ($x = 0$) is plotted in figure 9. The result of Prabhakar et al. [11], whose collocation penalty LSFEM leads to good mass conservation with this problem is also included as a reference. It is observed that the non-adaptive grid results in a maximum velocity that is considerably lower than the reference value. On the other hand, the adaptive grid results are in good agreement with Prabhakar et al. [11]. The mass flow rate obtained by integrating the velocity profiles over the cross section are 0.670 and 0.995 for non-adaptive and adaptive grids respectively. This indicates less than 1% mass loss with adaptive refinement. Figure 10 illustrates the centerline x-velocity, u_c plotted against x-coordinate in the upstream of the cylinder. A decay in the centerline velocity associated with a continuous mass loss is observed for the non-adaptive grid. On the other hand, the centerline velocity obtained by the adaptive grid increases towards the downstream, which is the expected behavior due to developing boundary layers near the channel walls.

Finally, figure 5.3 shows the distribution of element averaged least squares functional inside the channel. It is observed that p-type adaptive refinement strategy manages to keep the least squares functional between prescribed bounds i.e. [10^{-9}, 10^{-6}] by refining and unrefining accordingly. One exception is the elements adjacent to inflow boundary.

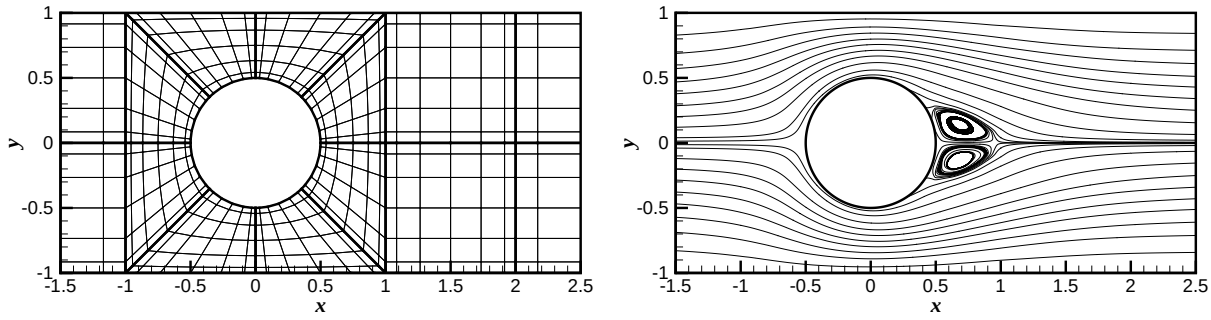

(a) Non-adaptive grid

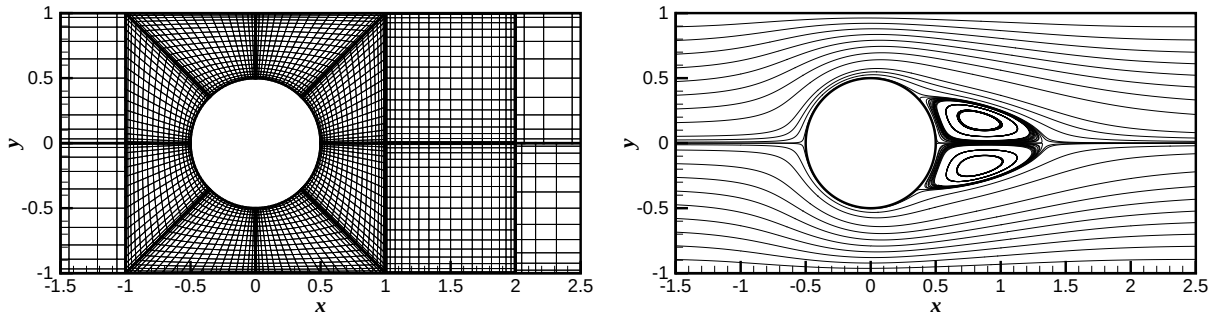

(b) Adaptive grid

Figure 8: Flow past a large cylinder: Computational grids and streamlines

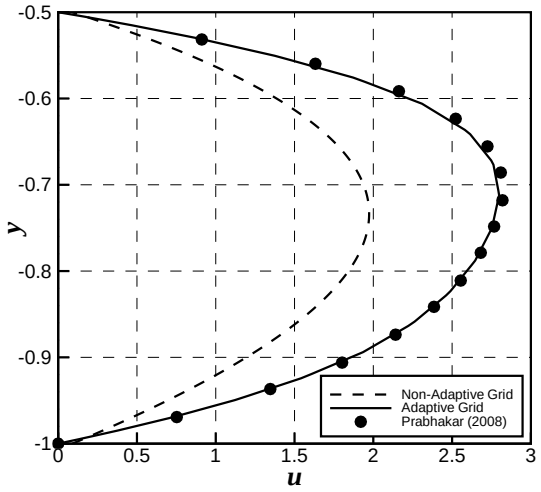

Figure 9: x-velocity profile taken from the vertical section between cylinder and lower channel wall, $x = 0$

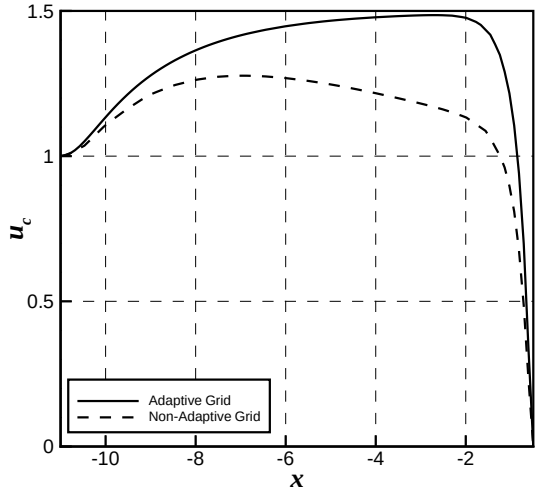

Figure 10: x-velocity profile taken from the horizontal section between upstream and cylinder, $y = 0$

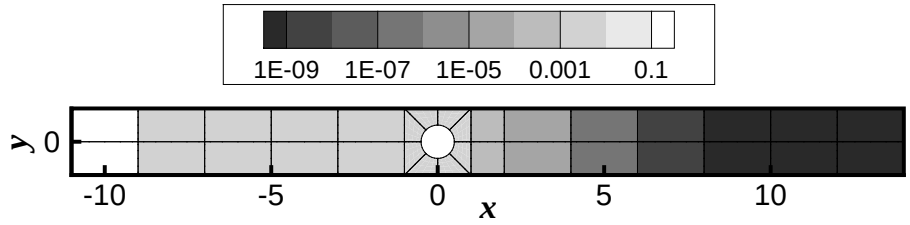

(a) Non-adaptive grid

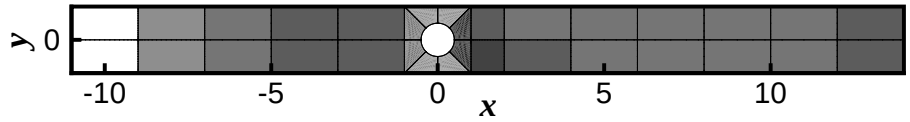

(b) Adaptive grid

Figure 11: Distribution of elemental least squares functional over the domain. Darker regions indicate lower errors.

However, those elements are exposed to singularities in x-velocity due to uniform inflow boundary condition near the channel walls. Favorable convergence characteristics of high-order methods disappear near such singularities[25]. A fully developed parabolic velocity profile at the inlet would be a physically more realistic boundary condition.

6 CONCLUSION

In this study, a laminar incompressible flow solver based on least squares spectral element method is introduced. The solver has the ability to work on non-conforming Cartesian grids and perform p-type adaptive refinement using least squares functional error estimate. This combination of the numerical method and grid structure is rare in both least squares and non-conforming Cartesian grid literature. It is shown that the solver achieves spectral convergence for smooth problems even in the presence of h and p-type non-conformities. 2-dimensional lid-driven cavity problem with corner singularities is also solved effectively by the virtue of local refinement abilities of the non-conforming Cartesian grid. Poor mass conservation performance of least squares spectral element method is illustrated by a channel flow with a large circular cylindrical obstacle. It is shown that the mass conservation can be improved by utilizing p-type adaptive refinement. As a result, poor mass conservation performance of least squares spectral element method may not be of practical concern when adaptive refinement is employed.

REFERENCES

[1] W. Coirier and K. Powell, "Solution-adaptive Cartesian cell approach for viscous and inviscid flows," *AIAA JOURNAL*, vol. 34, no. 5, pp. 938–945, MAY 1996.

[2] M. Aftosmis, M. Berger, and J. Melton, "Robust and efficient Cartesian mesh generation for component-based geometry," *AIAA JOURNAL*, vol. 36, no. 6, pp. 952–960, JUN 1998.

[3] T. Ye, R. Mittal, H. S. Udaykumar, and W. Shyy, "An accurate cartesian grid method for viscous incompressible flows with complex immersed boundaries," *Journal of Computational Physics*, vol. 156, no. 2, pp. 209 – 240, 1999.

[4] J. H. Bramble and A. H. Schatz, "Least squares methods for 2mth order elliptic boundary-value problems," *Mathematics of Computation*, vol. 25, no. 113, pp. 1–32, 1971.

[5] B. Jiang, *The Least-Squares Finite Element Method: Theory and Applications in Computational Fluid Dynamics and Electromagnetics*. Springer-Verlag, 1998.

[6] C. L. Chang and J. J. Nelson, "Least-squares finite element method for the stokes problem with zero residual of mass conservation," *SIAM Journal on Numerical Analysis*, vol. 34, no. 2, pp. 480–489, 1997.

[7] M. Proot and M. Gerritsma, "Mass- and momentum conservation of the least-squares spectral element method for the stokes problem," *Journal of Scientific Computing*, vol. 27, no. 1, pp. 389–401, Jun. 2006.

[8] P. P. Lynn and S. K. Arya, "Use of the least squares criterion in the finite element formulation," *International Journal for Numerical Methods in Engineering*, vol. 6, no. 1, pp. 75–88, 1973.

[9] J. M. Deang and M. D. Gunzburger, "Issues related to least-squares finite element methods for the stokes equations," *SIAM Journal of Scientific Computing*, vol. 20, no. 3, pp. 878–906, 1998.

[10] J. P. Pontaza, "A least-squares finite element formulation for unsteady incompressible flows with improved velocity–pressure coupling," *journal of computational physics*, vol. 217, pp. 563–588, 2006.

[11] Prabhakar, J. P. Pontaza, and J. N. Reddy, "A collocation penalty least-squares finite element formulation for incompressible flows," *Comput. Methods Appl. Mech. Engrg.*, vol. 197, pp. 449–463, 2008.

[12] J. N. Reddy, *An Introduction To The Finite Element Method*, 3rd ed. McGraw-Hill, 2006.

[13] A. T. Patera, "A spectral element method for fluid dynamics: Laminar flow in a channel expansion," *Journal of Computational Physics*, vol. 54, no. 3, pp. 468 – 488, 1984.

[14] R.-Y. Chang and C.-H. Hsu, "A variable-order spectral element method for incompressible viscous flow simulation," *International Journal for Numerical Methods in Engineering*, vol. 39, no. 17, pp. 2865–2887, 1996.

[15] C. Sert and A. Beskok, "Spectral element formulations on non-conforming grids: A comparative study of pointwise matching and integral projection methods," *Journal of Computational Physics*, vol. 211, no. 1, pp. 300 – 325, 2006.

[16] B.-N. Jiang and G. F. Carey, "Adaptive refinement for least-squares finite elements with element-by-element conjugate gradient solution," *International Journal for Numerical Methods in Engineering*, vol. 24, no. 3, pp. 569–580, 1987.

[17] B. N. Jiang and V. Sonnad, "Least-squares solution of incompressible navier-stokes equations with the p-version of finite elements," *Computational Mechanics*, vol. 15, no. 2, pp. 129–136, Nov. 1994.

[18] G. E. Karniadakis and S. J. Sherwin, *Spectral/*hp *Element Methods For Computational Fluid Dynamics*. OXFORD University Press, 2005.

[19] L. I. G. Kovasznay, "Laminar flow behind a two-dimensional grid," *Mathematical Proceedings of the Cambridge Philosophical Society*, vol. 44, no. 01, pp. 58–62, 1948.

[20] O. Botella and R. Peyret, "Benchmark spectral results on the lid-driven cavity flow," *Computers & Fluids*, vol. 27, no. 4, pp. 421 – 433, 1998.

[21] C.-H. Bruneau and M. Saad, "The 2d lid-driven cavity problem revisited," *Computers & Fluids*, vol. 35, no. 3, pp. 326 – 348, 2006.

[22] U. Ghia, K. Ghia, and C. Shin, "High-re solutions for incompressible flow using the navier-stokes equations and a multigrid method," *Journal of Computational Physics*, vol. 48, no. 3, pp. 387–411, 1982, cited By (since 1996) 901.

[23] T. Kattelans and W. Heinrichs, "Conservation of mass and momentum of the least-squares spectral collocation scheme for the stokes problem," *J. Comput. Phys.*, vol. 228, no. 13, pp. 4649–4664, 2009.

[24] W. J. Gordon and C. A. Hall, "Transfinite element methods: Blending-function interpolation over arbitrary curved element domains," *Numerische Mathematik*, vol. 21, no. 2, pp. 109–129, Apr. 1973.

[25] F. Auteri, N. Parolini, and L. Quartapelle, "Numerical investigation on the stability of singular driven cavity flow," *Journal of Computational Physics*, vol. 183, no. 1, pp. 1 – 25, 2002.